Diameter Tuning of Single-Walled Carbon Nanotubes with Reaction Temperature Using a Co Monometallic Catalyst

ARTICLE *in* THE JOURNAL OF PHYSICAL CHEMISTRY C · JUNE 2009

Impact Factor: 4.77 · DOI: 10.1021/jp903129h

5 AUTHORS, INCLUDING:

Xiaoming Wang
BASF SE
19 PUBLICATIONS **328** CITATIONS
SEE PROFILE

Fang Ren
Metropolitan Museum of Art
23 PUBLICATIONS **267** CITATIONS
SEE PROFILE

Diameter Tuning of Single-Walled Carbon Nanotubes with Reaction Temperature Using a Co Monometallic Catalyst

Nan Li, Xiaoming Wang, Fang Ren, Gary L. Haller, and Lisa D. Pfefferle*

Department of Chemical Engineering, Yale University, New Haven, Connecticut 06520

Received: April 5, 2009

Metal incorporated MCM-41 has proven to be a valuable template for the growth of narrow distributions of single-walled carbon nanotubes (SWNT), producing samples with a wide range of different mean diameters. The ability to obtain narrow diameter distributions at different mean diameters is important for applications that require particular (*n*,*m*) nanotubes. Another advantage of this system is the ease of cleaning and low metal content as compared to bimetallic systems. In this Article, we show that Co-MCM-41 allows diameter tuning of SWNT produced over a broad diameter range (from 0.6−0.8 to 1.8−2.0 nm) by changing reaction temperature. The lower temperature reaction provides a robust means to obtain very small diameter SWNT. X-ray absorption experiments show that the change in SWNT diameter correlates with the change in metal particle size.

1. Introduction

The unique electronic and mechanical properties of single-walled carbon nanotubes (SWNT) have made them attractive for a large number of applications. Electronic properties of SWNT depend on their diameter and chirality.[1] For the typical diameters at which SWNT are grown, there are about 100 different chiralities.[2] Progress on applications has been hindered by quality issues in commercial SWNT and/or lack of a commercially viable separation process. Small, <0.7 nm, diameter SWNT have very special properties including high temperature superconductivity, they are one of the strongest 1-D materials,[3] and they exhibit unusual, unpredicted electronic properties.[4−6] High curvature is associated with properties that vary dramatically with applied force enabling switches and nonvolatile memories. To date, however, no economically feasible methods exist for reliably preparing SWNT of a predetermined tube identity, either by selective synthesis or through postsynthesis separation.

Significant work has been directed toward obtaining a narrow distribution synthesis of SWNT. One area that we and others have worked on is the use of bimetallic systems[7−11] either to anchor ultrasmall particles of the SWNT growth catalyst[10] or to perturb its properties (e.g., providing a physical constraint,[7] acting as a carbon sink,[11] etc.). A drawback of these catalysts, however, is that purification of SWNT requires removal of two metals and can lead to increased impurities in the products, and the second metal is usually difficult to remove using routine chemical reagents (e.g., molybdenum carbide is highly refractory). The uncleaned metal catalyst residue can greatly affect the performance of SWNT for a large variety of applications, including, but not limited to, biotechnology,[12] microelectronics,[13] and catalysis.[14] Thus, a simple yet effective way to tune the SWNT diameter using easily removable monometallic catalysts is needed and not yet reported.

We have reported SWNT formed on subnanometer metal particles controlled by the framework of an amorphous mesoporous silica template, MCM-41.[15−22] The fact that the silica is amorphous is important because the chemistry of the wall can be altered independent of the pore structure. Our previous work used templates with 10−18 carbon atoms in the alkane portion of the surfactant used to template the MCM-41 corresponding to pore sizes from 1.8 to 3.1 nm. The pore diameter affects the reducibility of the metal in the silica framework with smaller pores resulting in higher reduction temperatures.[19] The 10-carbon alkane surfactant, C10, is different from other templates we have used because the pore size is smaller and the silica may be more mobile as evidenced by slightly lower stability of the silica framework. In a previous paper,[22] we characterized the C10 Co-MCM-41 catalyst and growth of carbon nanotubes over this catalyst. An interesting finding was that the yield based on carbon per catalyst weight (grams of carbon per gram catalyst) was extremely high (over 50%) as compared to other CVD processes using carbon monoxide (CO) as the carbon source and compared to the 10−20% yield observed for our larger pore diameter catalysts. The reaction also has very high selectivity toward SWNT (96%, as reported in ref 22), and the amorphous carbon species can be easily removed by burning in air at 300 °C.[25] Another observation of note was that the highest yield was obtained for catalysts synthesized at a lower pH (10.5 or 11) than for larger pore MCM-41. We theorized that the occlusion of the Co clusters by the silica of the MCM-41 framework (a physical constraint on particle growth) may be responsible for more smaller particles or domains.

We have previously observed that the reaction temperature causes a change in SWNT diameter distribution on Co-MCM-41 catalysts,[16] and similar results have been reported for $Co-Mo/SiO_2$ catalysts.[8] While this has not been generally reported for monometallic catalysts,[23] what the Co-MCM-41 and bimetallic systems such as $Co-Mo/SiO_2$ likely have in common is an anchoring mechanism between the active metal and the other catalyst components. The anchoring mechanism of Co metal particles to Co ions in the MCM-41 silica matrix is discussed in ref 18, and the anchoring of Co metal to MoC in the $Co-Mo/SiO_2$ catalyst is presented in ref 24. In this Article, we report a detailed study of "tuning" of the SWNT mean diameter distribution using a monometallic catalyst, by CO disproportionantion over C10 Co-MCM-41 under different reaction temperatures. Tube identity can be varied greatly by

* Corresponding author. E-mail: lisa.pfefferle@yale.edu.

10.1021/jp903129h CCC: $40.75
Published on Web 05/14/2009

operating at low temperature as compared to those normally used in CO disproportionation, and thus catalyst reaction temperature has a significant effect on the (*n*,*m*) identity of SWNT produced. In addition, at the very lowest temperature, very small SWNT were produced including 0.64 nm diameter. The SWNT synthesized in this method is very easy to clean, and the residue metal after simple base−acid washing[25] is less than 1%[22] (0.760% residue cobalt from inductively coupled plasma (ICP) results provided by Galbraith Laboratories, Inc.). The successful tuning of SWNT diameter distribution is due to the interaction between Co and the MCM-41 silica framework, and the detailed mechanism is explored by X-ray absorption spectroscopy (XAS) with other auxiliary methods.

2. Experimental Section

2.1. SWNT Synthesis Procedure. For the results reported here, we used a C10-MCM-41 template substituted with 3 wt % Co^{2+} having a mean pore diameter of 1.8 nm by the BJH method.[26] The catalysts used in this study were synthesized at a pH of 10.5 following the method described in ref 22.

SWNT was produced by catalytic disproportionation of CO flowing over a bed of the Co-MCM-41 catalyst maintained at constant temperature. Before CO disproportionation, pretreatment involving almost complete reduction of Co^{2+} was found in earlier studies to be important for both high yield and good selectivity.[22] Two hundred milligrams of catalyst was prereduced in pure hydrogen (99.999%, Airgas) for 30 min at temperatures ranging from 550 to 950 °C and then purged with Ar (99.999%, Airgas) for 5 min at the prereduction temperature. After prereduction, the catalyst was exposed to CO (99.99%, Airgas) flow, which first flowed through a carbonyl trap to eliminate Fe pentacarbonyl generated from reaction with the tank wall, at the various reaction temperatures from 550 to 950 °C at 80 psig for 30 min. Subsequently, the catalyst was cooled in flowing Ar to room temperature. The reactant flow rate in this study was fixed at one standard liter per minute.

2.2. Characterization Methods. SWNT in the product was analyzed by a variety of techniques including thermal gravimetric analysis (TGA), Raman spectroscopy, fluorescence spectroscopy, UV−visible−near-infrared (UV−vis−NIR) spectroscopy, and transmission electron microscopy (TEM). The study of Co particle size was conducted using X-ray absorption spectroscopy (XAS).

Thermogravimetric Analysis (TGA). TGA data on each as-synthesized sample were collected on a Setaram Setsys 1750 instrument. Around 15 mg of as-synthesized sample was loaded in an alumina crucible and then heated to 200 at 10 °C/min and held at 200 °C for 30 min in air (ultra zero grade, Airgas) flow to remove moisture from the sample. The data of sample weight versus temperature were recorded during the two successive temperature ramps from 200 to 1000 °C at 10 °C/min and holding at 1000 °C for 1 h. The second set of data in air flow was used as a baseline for the first to minimize the influence of crucible buoyancy and drag force, which are a function of temperature.

Raman Spectroscopy. Raman spectra of as-synthesized SWNT samples, without purification, were collected on a Jasco NRS-3100 laser Raman spectrometer with excitation wavelengths of 488, 532, and 785 nm.

Fluorescence Spectroscopy. One milligram of SWNT, silica framework removed, was dispersed in 40 mL of 1 wt % sodium dodecyl sulfate (SDS, >99%, Pierce) aqueous solution and then sonicated in a tip sonicator (S3000-001, Misonix) at 30 W for 1 h. After sonication, the suspension was centrifuged at 47 000*g* for 1 h, and then about 1 mL of supernatant on the top was decanted for fluorescence measurement. The fluorescence data were collected by a NS1 NanoSpectralyzer spectrofluorometer with an IGA (InGaAs) NIR detector at three excitation wavelengths of 638, 681, and 784 nm. To confirm the fluorescence results, some of the samples in this study were also analyzed by photoluminescence (PL) mapping on a Jobin-Yvon Nanolog3 spectrofluorometer with an IGA NIR detector, where the sample was prepared in a similar way: 0.5 mg of silica removed sample was dispersed in 10 mL of 1 wt % sodium dodecyl benzene sulfonate (SDBS, 99%, Sigma)/D_2O (99.9% atom D, Sigma) solution and then sonicated in a tip sonicator (SONICS, VCX-130) at 80% amplitude for 1 h; the suspension was then centrifuged at 100 000*g* for 1 h, and 80% of the supernatant was decanted for measurement.

UV−Visible−Near-Infrared (UV−Vis−NIR) Spectroscopy. The UV−vis−NIR measurement was performed on a Varian Cary 5000 UV−vis−NIR spectrometer. The sample for this measurement was prepared in the same way as for PL measurement described above.

Transmission Electron Microscopy (TEM). TEM images of both as-synthesized and silica-removed SWNT samples were recorded on a Philips Tecnai 12 electron microscope operated at 120 kV. One milligram of the sample was dispersed in anhydrous ethanol by a bath sonicator (B300, Branson) for 1 h, and one drop of this suspension was applied to a TEM grid with holey carbon film following by drying in air for about 30 min.

X-ray Absorption Spectroscopy (XAS). The XAS data in this Article were collected at beamlines X18B, X23A2, and X23B at the National Synchrotron Light Source (NSLS), Brookhaven National Laboratory. One hundred milligrams of fresh catalyst or as-synthesized sample was pressed into a round, free-standing pellet with the approximate thickness of 0.5 mm. The pellet was loaded into a stainless steel reactor with gas flow and precise temperature control to perform in situ reduction. The detailed description of this reactor can be found in ref 16. Extended X-ray absorption fine structure (EXAFS) spectra were recorded in the transmission mode from 200 eV below to 600 eV above the Co K edge (7709 eV). A Co foil (4 μm thick) was used as an internal reference to calibrate the edge energy of each sample analyzed.

3. Results

3.1. Catalyst Prereduction Temperature. A study of the effect of catalyst prereduction on SWNT diameter tuning was conducted using C10 3 wt % Co-MCM-41 as catalyst. The catalyst was prereduced in hydrogen at different temperatures from 550 to 950 °C and then all reacted at 750 °C. Figure 1 shows the carbon yield of nine samples prereduced at different temperatures from 550 to 950 °C as a function of prereduction temperature. Here, the yield, determined by TGA, is defined as the mass of carbon over the mass of catalyst used. The yield reaches its maximum (over 50%) at 750 °C and decreases when prereduction temperature moves toward lower and higher temperatures. The inset of Figure 1 shows the Raman spectrum at 785 nm excitation wavelength of the as-synthesized sample prereduced at 750 °C, which represents a typical Raman spectrum of all these samples. The Raman spectrum between 40 and 400 cm^{-1}, which is usually called the radial breathing mode (RBM), was used to determine the tube diameter of SWNT. All of these samples show almost identical Raman spectra at an excitation wavelength of 785 nm, indicating no significant diameter change via the change of prereduction

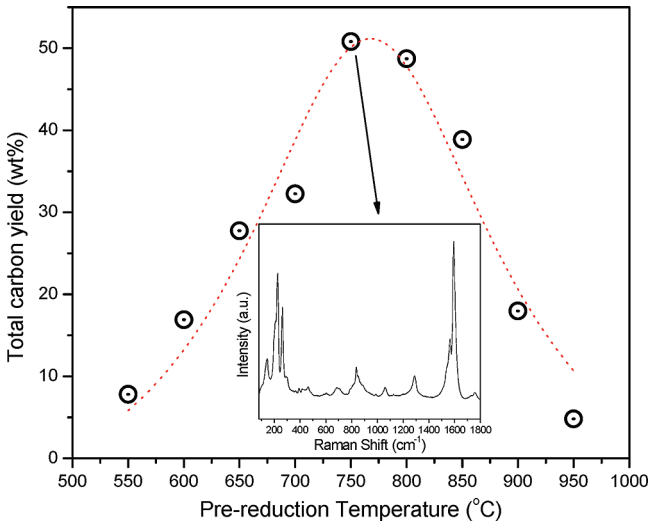

Figure 1. Total carbon yield as a function of prereduction temperature with reaction at 750 °C. The inset shows the Raman spectrum for the as-synthesized SWNT prereduced at 750 °C and reacted at 750 °C.

temperature combined with TEM (see Figures S1 and S2 in the Supporting Information).

The yield drops at lower temperatures due to the incomplete prereduction of Co resulting in fewer Co particles that can be utilized to grow SWNT, which is illustrated in Figure 2. Figure 2a shows the X-ray absorption near-edge structure (XANES) spectra of the fresh catalyst, the catalyst reduced at 550 °C, and the catalyst reduced at 750 °C, in comparison with a Co metal foil. Both the pre-edge peak at around 7709 eV and the white line at around 7725 eV indicate that the Co species in the catalyst remain mostly oxidized after prereduction at 550 °C for 30 min, but become almost completely reduced after exposure to hydrogen at 750 °C for 30 min. That is, the pre-edge peak of the 750 °C catalyst is indistinguishable from the Co foil, but the white line and the post-edge are different. Most of this difference, for example, the interference modulation, has to do with the Co small particle size relative to the foil, but may also have a contribution from unreduced Co cations. This can be further demonstrated when looking at the *R* space spectra in Figure 2b, in which the catalyst reduced at 550 °C shows mainly Co−O bonding with less evidence of Co−Co bonding. The catalyst reduced at 750 °C, however, shows only Co−Co bonding with no observable Co−O bonding. The lower intensity of the Co−Co peak for the catalyst reduced at 750 °C than the peak of Co foil implies that the Co here in the catalyst is in a nanoconfined environment. Therefore, when changing the prereduction temperature from 550 to 750 °C, the catalyst changes from partially reduced to complete reduction within the measurement limits of X-ray absorption spectroscopy. Because only metallic Co is an effective catalyst for SWNT synthesis, the yield increases with increased prereduction temperature from 550 to 750 °C. However, when the prereduction temperature increases above 750 °C, the carbon yield decreases because of sintering to larger Co clusters. It should be noted that the diameter of the SWNT remains unchanged while changing the prereduction temperature, which will be discussed below.

3.2. SWNT Diameter Tuning Using Reaction Temperature. The prereduction temperature was fixed at 750 °C when studying the reaction temperature effect because it produced the highest yield (as shown in Figure 1) when using a 750 °C reaction temperature. This may not be the overall optimum when a different reaction temperature is used. Several experiments (not shown here) were also run at lower prereduction temperature (550 °C) to test the effect on nanotube identity. In these experiments, the tube identities observed for each reaction temperature studied were similar to that for the 750 °C prereduction temperature, but the yield was significantly lower.

As shown in Figure 3, the yield obtained for all reaction temperatures was above 6% and reached over 50% at temperatures between 700−800 °C. Unlike for the case of changes in prereduction temperature, the change in reaction temperature resulted in a significant shift in the diameter of nanotubes formed as shown by Raman, fluorescence, and TEM. Figure 4 shows the Raman spectra taken at 785 nm excitation wavelength showing a shift in the tube diameter. When reacted at 950 °C, the major RBM peak is at 139 cm^{-1}, which corresponds to the tube diameter of 1.8 nm, as suggested by the theoretical work on SWNT Raman spectra.[27] When the reaction temperature is lowered, another peak at 227 cm^{-1} (1.1 nm) emerges and gradually becomes dominant at 800 °C. As the reaction temperature is lowered further to 750 °C, the 263 cm^{-1} (0.9 nm) peak becomes comparable to the 1.1 nm peak, and when the reaction temperature is below 650 °C, the 370 cm^{-1} (0.64 nm) RBM peak appears and becomes the majority species at 550 °C.

Notice that along with the 0.64 nm peak, some new intermediate frequency modes (IFM)[28−33] show up between 700 and 1200 cm^{-1} at reaction temperatures below 700 °C. To explore whether these strong IFM features are related to some new carbon species, a series of experiments were designed. The inset of Figure 5 shows the derivative thermogravimetric (DTG) pattern of the TGA results of the sample reacted at 550 °C, which gives two peaks at 350 and 520 °C, respectively. The sample was heated at different temperatures in air and then subjected to Raman measurement, as shown in Figure 5. Oxidation as low as 250 °C increases the intensity of the RBM and IFM relative to the G band at ∼1600 cm^{-1}, presumably a result of modest oxidation of amorphous carbon. Oxidation at 420 °C and below (the position in between the two DTG peaks) causes no obvious change in Raman spectra, except a modest decrease of the 0.64 nm peak and the IFM peak intensities relative to the G band. However, when the temperature was further increased to 600 °C, which burns the majority of the tubes leaving the largest tubes in the sample, both the 0.64 nm peak and the intermediate features disappear together, indicating they are correlated, which is also in agreement with the theoretical prediction of IFM (between 600 and 1400 cm^{-1}) by many groups.[28−33] In addition, note that it is the smaller tubes that are preferentially destroyed by oxidation. The SWNT still remaining after exposure to air at 600 °C were those with the largest tube diameter detectable at the 785 nm excitation wavelength. We expected this from the argument that reactivity increases with the increase of tube curvature due to the strain of the sp^2 bonding. The SWNT diameter shifts in Raman spectra at other excitation wavelengths (488 and 532 nm) are also consistent with what is shown at 785 nm (see Figure S3 in the Supporting Information).

The TEM images of a series of as-synthesized samples at different reaction temperatures shown in Figure 6, consistent with the Raman data, show a clear shift in SWNT diameter with reaction temperature: the 550 °C sample mostly consists of the 0.6−0.7 nm tubes; the tubes in the 750 °C sample are mostly around 1 nm; while the majority in the 950 °C sample are around 2 nm. Note also that these TEM images were taken before the metal was removed from the sample showing that good dispersion was achieved at all conditions. The TEM images

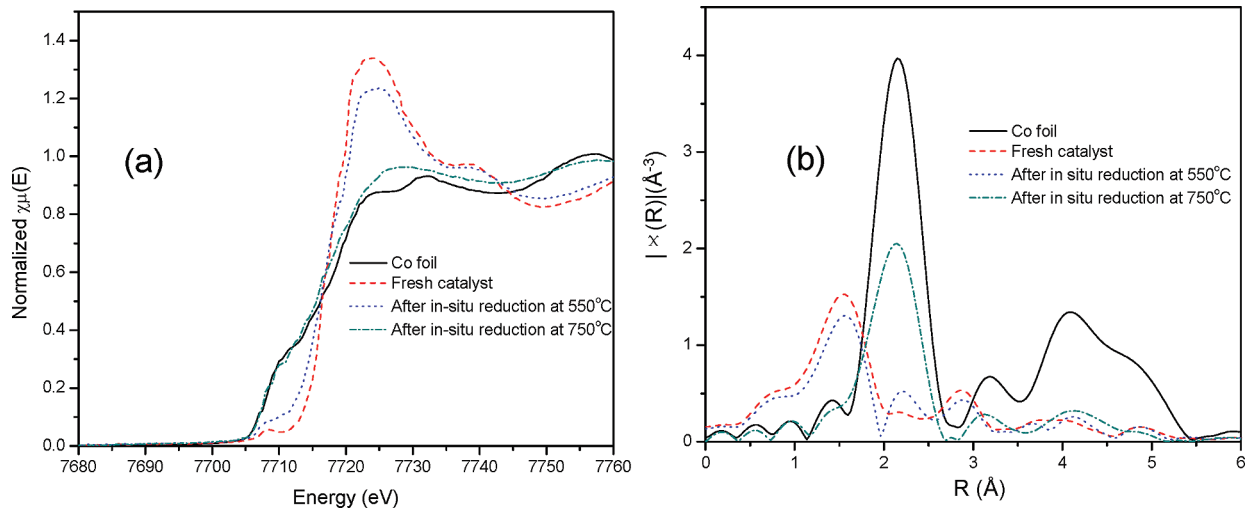

Figure 2. (a) Normalized XANES spectra near the Co K edge and (b) the k^2-weighted EXAFS data in R space for the catalyst after in situ reduction at 550 and 750 °C in comparison with the Co foil and fresh Co-MCM-41 catalyst.

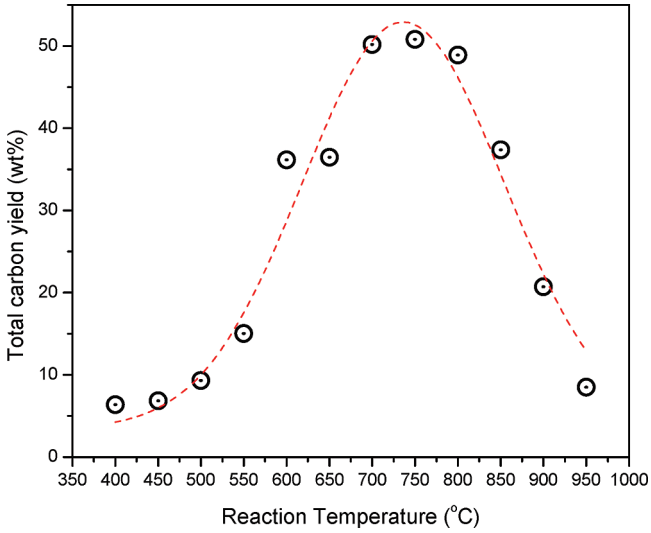

Figure 3. Total carbon yield as a function of reaction temperature following prereduction at 750 °C.

show little evidence for large metal particles except at the 950 °C reaction temperature. TEM images of five SWNT samples (with reaction temperatures from 550 to 950 °C) after silica removal but prior to cobalt particles removal also show a significant progression in tube diameter (see Supporting InformationFigure S4).

Figure 7 shows the raw fluorescence data for three excitation wavelengths for five SWNT growth temperatures from 550 to 950 °C. The fluorescence data show the same trend toward smaller tube diameters as the reaction temperature decreases with a peak out of the detectable regime at the lowest reaction temperature producing the smallest tubes. The difference in mean diameter and diameter distribution at each reaction temperature is dramatic. The lowest reaction temperatures show very small tubes (the smallest accessible using our fluorescence equipment is the (6,5) tube, but a peak on the edge of our detection limit is also observed). Many of the tubes grown at the highest reaction temperature are not shown as they are not accessible with our system, which has a cutoff of 1.4 nm in SWNT diameter. UV−vis−NIR spectra of these five SWNT samples also show that the SWNT diameter shifts toward larger tubes when increasing the reaction temperature (see Figure S5 in the Supporting Information).

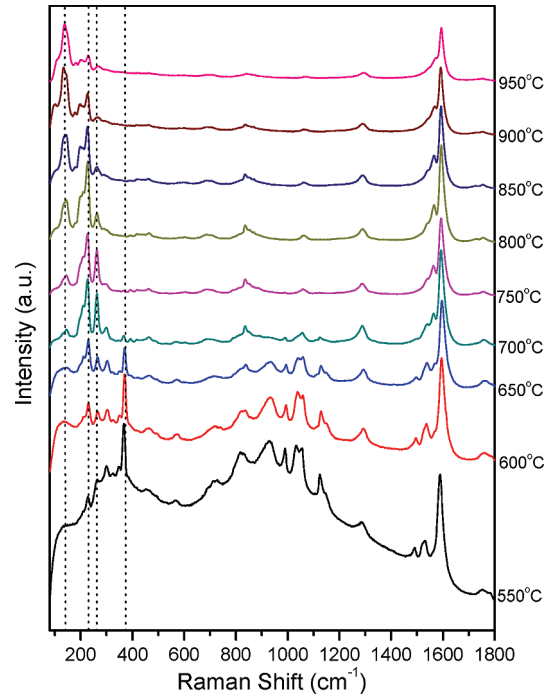

Figure 4. Raman spectra at excitation wavelength 785 nm for the as-synthesized SWNT samples prereduced at 750 °C and reacted at temperatures from 550 to 950 °C.

Photoluminescence (PL) intensity maps of SWNT produced at temperatures from 550 to 950 °C were also obtained as shown in Figure 8. The measurement was performed with a tunable excitation wavelength from 500 to 800 nm, and the emission was collected from 900 to 1350 nm. Each spike in the map represents a transition pair from an individual semiconducting (n,m) SWNT.[34,35] Roughly, the SWNT becomes larger in diameter as the peak moves from the lower excitation and emission corner toward the higher excitation and emission corner. This map can only show SWNT smaller than 1.3 nm in diameter due to the limitation of the detector. The PL map shows a very narrow distribution of SWNT identities at lower reaction temperatures where small tubes are dominant. The (6,5) tube is dominant in the SWNT sample reacted at 550 °C. Its intensity decreases as reaction temperature goes up and almost disappears at higher temperatures of 850 and 950 °C. The intensities of (7,5), (7,6), and (8,4) are quite weak at 550 °C and become

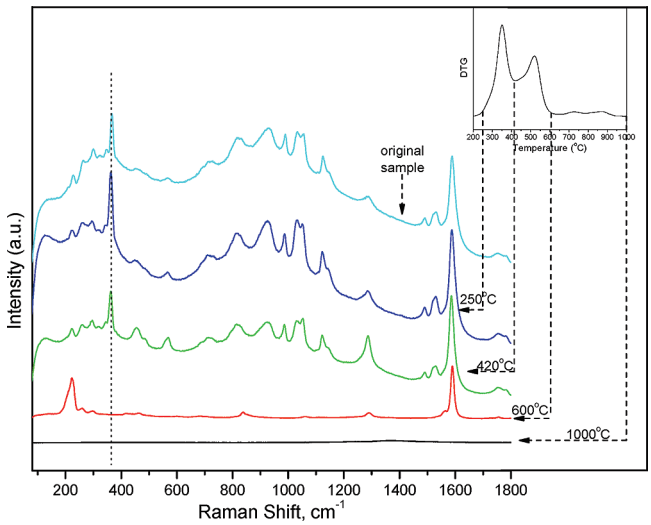

Figure 5. Raman spectra for the as-synthesized SWNT sample prereduced at 750 and reacted at 550 °C after oxidation in air for 30 min at the shown temperatures.

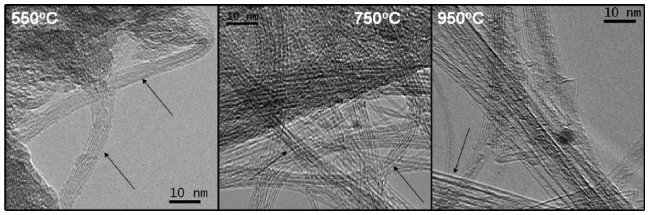

Figure 6. TEM images for the as-synthesized SWNT samples reacted at temperatures from 550 to 950 °C.

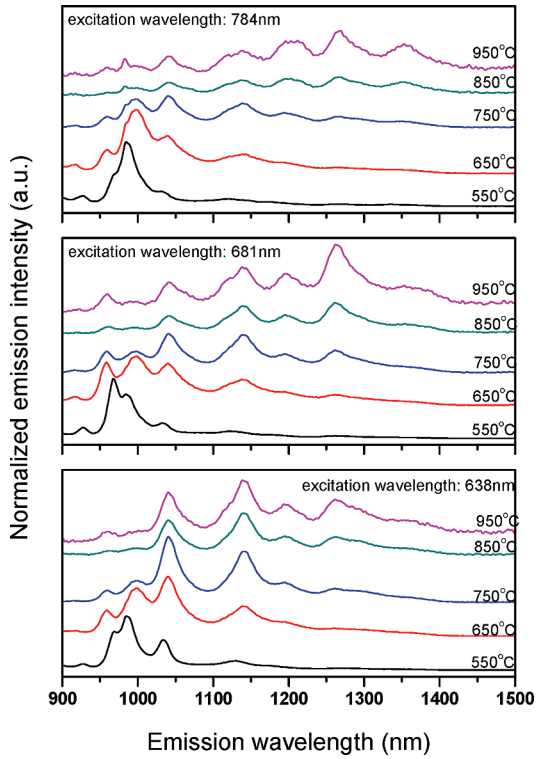

Figure 7. Multiexcitation fluorescence spectra for silica-removed SWNT prereduced at 750 °C and reacted at temperatures from 550 to 950 °C.

stronger on the 650 °C map. Finally, (7,5), (7,6), and (8,4) become dominant at 750 °C and then fade away as the temperature is increased to 950 °C. Note that at the highest temperature, Raman data and TEM images suggest that the tube diameters are mostly in a larger diameter range than covered by this technique.

X-ray absorption spectroscopy (XAS) analysis was carried out on the catalyst samples after reaction. Although this is a bulk analysis technique and volume averages over particle sizes, there is a clear trend of reduction in particle size as the reaction temperature is decreased. In the following section, XAS was used to study the mechanism of the diameter tuning, in combination with other techniques.

4. Discussion

4.1. Control of Co Particle Size by Changing Reaction Temperature. The change in SWNT diameter with reaction temperature is caused by the competition between particle growth and SWNT growth rates. An important feature of the C10 Co-MCM-41 catalyst is that hydrogen prereduction can be carried out at higher temperatures than for our larger pore catalysts while still obtaining high dispersion. This is evidenced both in temperature-programmed reduction (TPR) data and in our in situ X-ray absorption experiments during catalyst reduction under flowing hydrogen. Most of the actual catalyst particle formation occurs during the reaction step under CO[18] as we see from the XAS results discussed below.

The XAS spectra of Co in the catalyst with the as-synthesized SWNT produced at different reaction temperatures are shown in Figure 9. The XANES spectra in Figure 9a show that the pre-edge peak and the white line intensity of the sample reacted at 950 °C are very close to the Co foil, while all of the others are partially reduced, and the lower is the reaction temperature, the higher is the white line intensity. The *R* space spectra in Figure 9b provide information on the average Co−Co coordination number. As the reaction temperature increases from 550 to 950 °C, the intensity of the Co−Co peak also increases, indicating the increase of average Co−Co coordination number; thus, higher reaction temperature leads to larger Co nanoparticles.

To quantitatively study the XAS spectra, *R* space fitting was carried out via IFEFFIT software package,[36] using standard Co and Co_3O_4 structures (calculated from FEFF 6.0[37]) to determine the average first shell coordination number of the Co particles. The spectrum of Co foil was used to determine the amplitude function and the phase shift, assuming it has hcp stacking crystallographic structure, which is the same as the bulk Co structure. The fitting results are listed in Table 1.

The fitting results show that from 550 to 950 °C, the average Co−Co coordination number increases, which can also be observed in Figure 9b. The average size of the Co nanoparticle can also be estimated from the average first shell coordination number using Calvin's model.[38] The particle size estimation is listed in Table 1 and plotted over reaction temperature in Figure 10, and the corresponding TEM pictures are also shown in Figure 10. It can be observed that the particle size from EXAFS and from TEM fit very well, and also the particle size and the corresponding carbon nanotube diameter match well.

Thus, tuning of the SWNT diameter is correlated well with control of the Co particle size by the reaction temperature. In the following, we will discuss the mechanism for the particle size control leading to the diameter shift. However, before moving to the next discussion point, it should be pointed out that all of the samples studied in this section were prereduced in hydrogen at 750 °C before reaction: Figure 2 shows that the Co was almost completely reduced at this stage. So, what causes the difference in the white line intensity in Figure 9a? Actually we have encountered the same situation when studying the effect

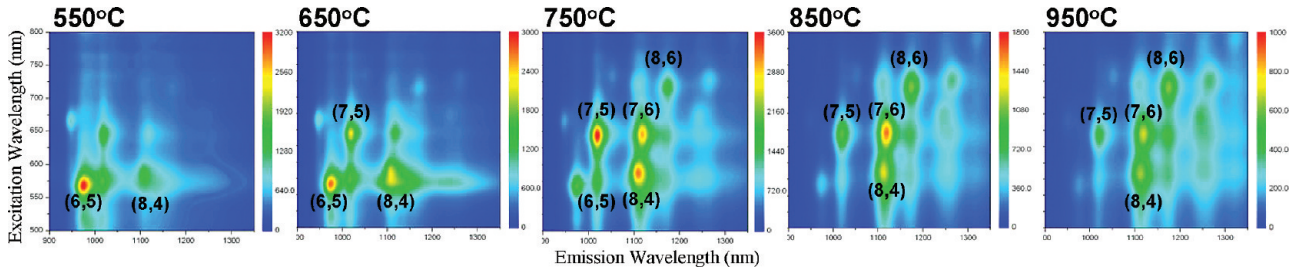

Figure 8. Photoluminescence (PL) intensity maps for silica-removed SWNT prereduced at 750 °C and reacted at temperatures from 550 to 950 °C.

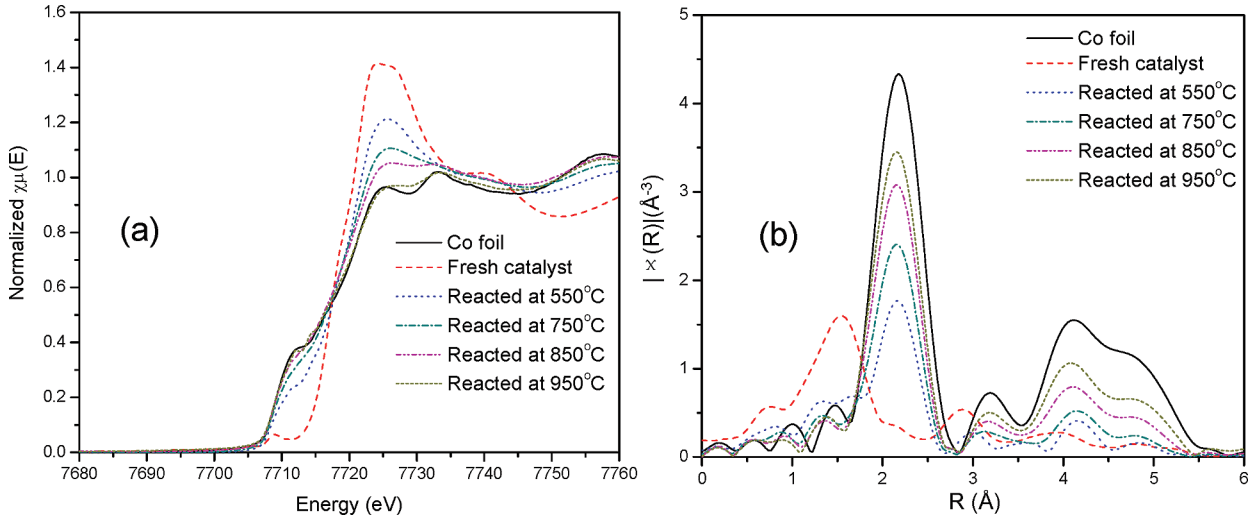

Figure 9. (a) Normalized XANES spectra near the Co K edge and (b) the k^2-weighted EXAFS data in R space for the as-synthesized SWNT samples prereduced at 750 °C and reacted at temperatures from 550 to 950 °C in comparison with the Co foil and fresh Co-MCM-41 catalyst.

TABLE 1: EXAFS Fitting Results for the As-Synthesized SWNT Samples Prereduced at 750 °C and Reacted at Temperatures from 550 to 950 °C

reaction temperature (°C)	coordination number (Co−Co)	cluster size diameter (nm)	number of atoms
550	5.87 ± 0.13	0.70	16.2
750	7.94 ± 0.14	1.09	59.7
850	9.52 ± 0.29	1.80	226.6
950	10.25 ± 0.67	2.56	556.2

of CO pressure on this reaction. In situ XANES results show that when changing CO pressure, the white line intensity does not change much, and almost all of the Co still remains in the reduced state.[18] However, when taking EXAFS measurements on the as-synthesized products (which were stored in the lab for a long time before measurement), the products from different CO pressure show quite different white line intensity, and some of them are highly oxidized.[17] A likely reason is that the Co particles were partially reoxidized when exposed to air. Because the reoxidization can only occur at the outer surface of the particles, the degree of oxidation can be used as a consistency check of the calculated particle size. Therefore, the product from 550 °C, with the highest white line, has the smallest particle size, and vice versa, which is consistent with the results from the diameter fitting. An alternative interpretation of the line intensity is that it reflects some degree of surface carbide formation, another kind of Co oxidation, for example, Co + 2CO → CoC + CO_2. We have chemical evidence for surface carbide; that is, Co is difficult to dissolve by HCl, but after a mild oxidation, most of the Co can be dissolved by HCl.[25] Moreover, this kind of incorporation of the metal catalyst into carbon has been previously reported for the Ni−carbon nanofiber system by EXAFS and XANES,[39] which suggests that the dominant species in the as-synthesized sample after exposure to air is oxide, while the existence of carbide can be observed after the removal of oxides. Most likely there are contributions from both surface oxide and carbide to the spectra shown in Figure 9, but the majority is likely surface oxide from air oxidation.

4.2. Mechanism for Particle Size Control. In our previous study, two mechanisms, anchoring and occlusion, have been shown to be effective in Co particle size control in the Co-MCM-41 system.[21] Direct anchoring has been ruled out because this mechanism is observed to be effective when some of the metal ions exist near the surface of the silica wall. In contrast, in our case Co is completely reduced, and negligible anchoring sites are left in the silica wall. Even so, the catalyst particles remain highly dispersed as evidenced by the Co−Co coordination number reported in Table 1. Occlusion may be the major controlling factor for the particle size and thus the SWNT diameter control. Previous research shows that, although hydrogen can reduce Co^{2+} ion to metallic Co, the Co does not move out of the silica wall easily, and thus it is "occluded" in the surface, either atomically dispersed[17,20] or in the form of small Co clusters.[20] In our case, it is probably small clusters rather than atomically dispersed Co, because the Co−Co bond is evident in Figure 2b after hydrogen prereduction but before reaction. On the other hand, the introduction of CO enhances the migration of metallic Co on the surface of the MCM-41 pores; thus, the final formation of Co particles is in the CO reaction stage.[16−18,20,21] Here, we propose the mechanism that the size of the Co particle is determined by the competition between the aggregation of small Co clusters and the deposition

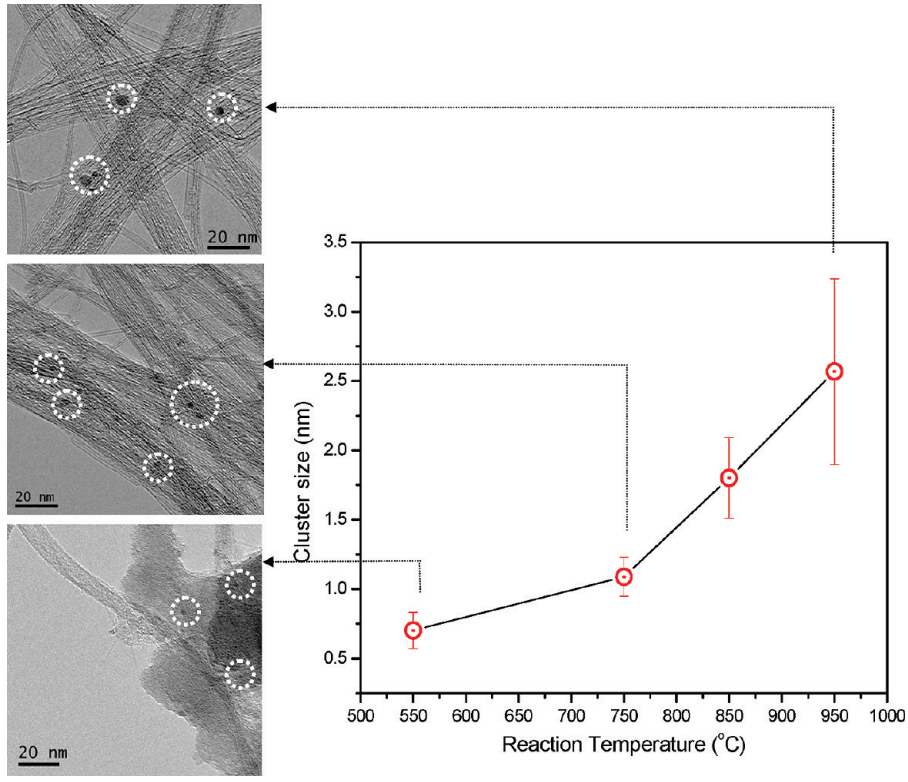

Figure 10. Cobalt cluster size determined by EXAFS fitting in as-synthesized SWNT samples reacted at temperatures from 550 to 950 °C and TEM images indicating cluster size.

of carbon on Co particles to produce SWNT. The aggregation of Co clusters is temperature sensitive, which can also be concluded from Table 1 where the average Co−Co coordination number increases from 5.87 to 10.25 when reacted at temperatures from 550 to 950 °C. At low temperature, the mobility of the Co cluster is very low, and thus aggregation is lessened, and then CO reaction takes place on these small clusters or small aggregates, leading to small diameter SWNT with a narrow diameter distribution, as for the sample reacted at 550 °C. At very high temperature, the aggregation of Co clusters becomes the fast step and forms large Co particles very rapidly, followed by the SWNT growth, so the SWNT produced has a large diameter and relative narrow distribution, like the sample reacted at 950 °C. At medium temperatures (between 600 and 900 °C), the aggregation of Co into larger clusters and the growth of SWNT on already-formed Co clusters are comparable and compete with each other, leading to the SWNT with a wider diameter distribution as compared to the very low and very high temperature cases, and the mean diameter is in between, as shown in Figures 4, 6, 7, 8, S3, S4, and S5.

4.3. Verification of the Mechanism. ***4.3.1. Evidence from Co Atom Mass Balance.*** The average number of Co atoms within the wall of one MCM-41 pore can be estimated using the following equation:[15]

$$N_{Co} = \frac{1}{2}\pi[(\frac{OD}{2})^2 - (\frac{ID}{2})^2]L\rho MA_N$$

where N_{Co} is the number of Co atoms per MCM-41 pore, OD and ID are the outer and inner diameters of the MCM-41 pore, determined by XRD and nitrogen physisorption, respectively, L is the pore length (about 100 nm), ρ is the density of silica (2.2 g/mL), M is the total number of moles of Co atoms per unit mass of catalyst, and A_N is Avogadro's constant. For the C10 Co-MCM-41 catalyst used in this study, the N_{Co} is calculated to be around 200.

The average number of Co atoms in a Co particle can be estimated from the Co cluster size, and the result is listed in Table 1. When comparing the average number of Co atoms in Co particles with the N_{Co} number, one can deduce that the Co particle after reaction at 550 °C contains only about 16 Co atoms. Thus, it is probably formed within the MCM-41 pore, and the diameter of SWNT grown at this temperature is very small. The sample reacted at 750 °C also has a smaller Co atom number than the N_{Co} number, so the majority of the SWNT grown at this temperature are of 0.9 and 1.1 nm diameter, which is smaller than the MCM-41 pore. On the contrary, the Co particle after reaction at 950 °C contains about 550 Co atoms, much larger than the N_{Co} number. Such large particles cannot be obtained during the hydrogen prereduction stage (because Co migration rate is low under a hydrogen atmosphere), but have to form from the aggregation of small Co clusters during the exposure to CO. The SWNT from 950 °C is mainly 1.8 nm. Taking into account the size of the carbon atom (about 0.34 nm),[40] the outer diameter of the SWNT is even larger than the MCM-41 pore, and thus they have to be outside the pore. The sample reacted at 850 °C has Co atom numbers comparable to those of the N_{Co} number, so the SWNT are made up of 1.1 and 1.8 nm tubes, on average, comparable to the diameter of the MCM-41.

The DTG pattern of the TGA data can also illustrate this, as shown in Figure 11, in which most of the curves have two DTG peaks, while only those reacted at 450 and 950 °C have one DTG peak. It has been observed that the temperature of burning is affected by the SWNT diameter, location of SWNT, catalyst particles, and heat transport,[22] which explains why some of the DTG patterns have one peak while the others have two with the two peaks at somewhat different temperatures. The SWNT grown at 950 °C has only one DTG peak on the high temperature side. Because in this sample, tubes are quite large

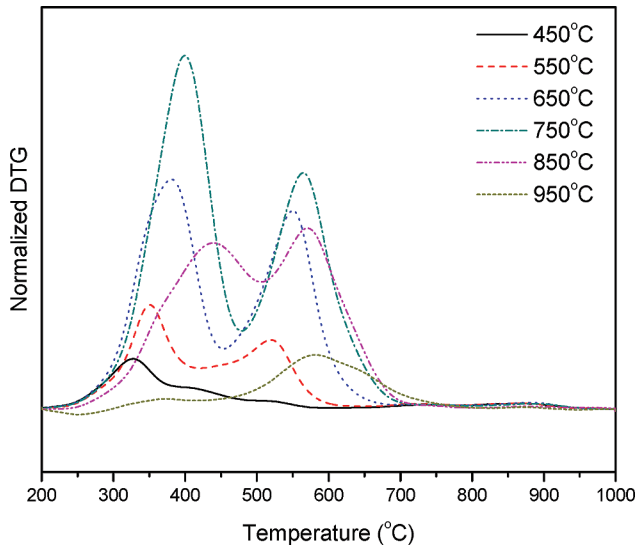

Figure 11. Derivative thermogravimetric (DTG) patterns normalized by catalyst weight for the as-synthesized SWNT samples prereduced at 750 °C and reacted at temperatures from 450 to 950 °C.

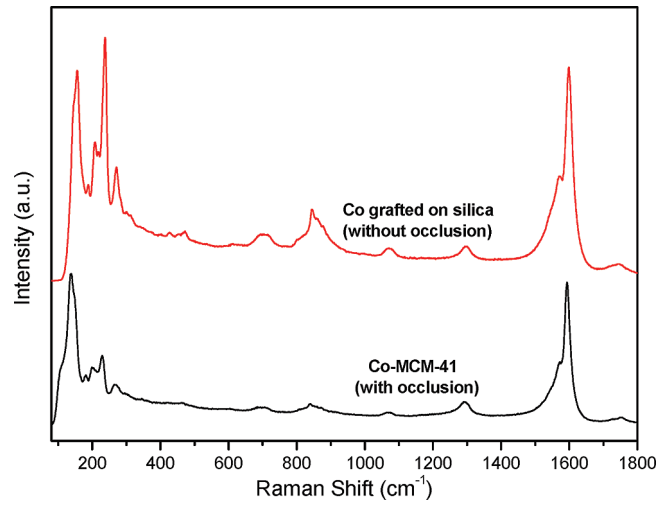

Figure 12. Raman spectra at excitation wavelength 785 nm for the as-synthesized SWNT samples prereduced at 750 °C and reacted at 950 °C using catalysts with and without occlusion.

in diameter and almost all of the SWNT are grown outside the MCM-41 pore, it is likely that this peak corresponds to the large SWNT outside the pore, while the lower temperature peak is the SWNT inside the pore. It should be noted that even if the Co particle is located inside the pore, it is still possible that the SWNT grows long enough to reach the outside of the pore (such is the case at 550 or 750 °C); thus the DTG pattern still has two peaks. Only at very low temperature, such as 450 °C, is the SWNT growth rate so low that the majority of the carbon nanotubes are confined to the pore, showing one single peak on the low temperature side. The assignment of DTG peaks can also be verified by the DTG pattern of SWNT grown from nonstructured silica, which shows one single DTG peak on the high temperature side.

By counting the Co atoms, we find that the Co particles after SWNT growth at 950 °C contain many more Co atoms than a single MCM-41 pore can accommodate based on a mass balance; thus the Co cluster aggregation must have occurred during the CO reaction stage, which provides indirect evidence for our mechanism. This is also consistent with the EXAFS results that the Co cluster size is determined after exposure to CO.

4.3.2. Evidence from a Catalyst Designed To Minimize Occlusion. As discussed above, we have proposed the mechanism that the tuning of SWNT diameter is due to the competition between the aggregation of Co clusters and the growth of SWNT, and amorphous silica occlusion plays an important role. To further verify the mechanism, another catalyst was synthesized by chemically grafting Co^{2+} ions at the outer surface of silica. Occlusion is less likely to occur in this catalyst. The detailed catalyst synthesis procedure has been described elsewhere.[41] The reduction pattern of this catalyst, as characterized by in situ XAS during reduction, is very similar to the reduction pattern of Co-MCM-41, as seen in Figure S6. The SWNT diameter obtained from this catalyst is similar to that from Co-MCM-41 at low temperature, because carbon deposition and SWNT growth dominate at such temperature and occlusion does not affect SWNT synthesis significantly. However, at high reaction temperature, as shown in Figure 12, when aggregation becomes rapid, the surface grafted catalyst gives much broader SWNT diameter distribution than does the Co-MCM-41 catalyst, where Co was isomorphously substituted inside the silica framework. The reason is that for Co-MCM-41, the Co clusters were occluded inside the silica so that SWNT growth is impossible at the initial stage, and to grow SWNT, they have to move out of the silica framework first, while at high temperature, the fast aggregation during this step makes the majority of Co clusters very large when the SWNT growth starts. On the other hand, the grafted catalyst can begin growth of SWNT right after CO is introduced, so the SWNT diameter is relatively broad, because of the coexistence of SWNT growth and Co aggregation.

5. Conclusions

The diameter of SWNT produced from carbon monoxide disproportionation over C10 Co-MCM-41 can be simply engineered by changing the reaction temperature. The SWNT diameter shifts systematically from 0.6−0.8 to 1.8−2.0 nm as the reaction temperature increases from 550 to 950 °C, verified by TEM, Raman, fluorescence, and UV−vis−NIR spectroscopies. The control of SWNT diameter is achieved via the control of Co particle size in this two-stage reaction. After almost complete prereduction under hydrogen, the Co particle size is finally determined by the CO reaction stage, due to the occlusion effect in the prereduction step. Carbon monoxide facilitates the migration of small Co clusters and brings them to the surface of MCM-41 pore wall. The competition between the Co aggregation and carbon deposition determines the size of the Co nanoparticle, which in turn determines the diameter of SWNT. The diameter distribution of SWNT synthesized from Co grafted catalyst also supports that occlusion is the key issue to control the particle size and diameter. SWNT produced by this method has extremely high surface area,[22] and the Co particle and MCM-41 catalyst can be easily removed,[25] which suggests many promising applications in various fields.[42,43]

Acknowledgment. We thank the Department of Energy (Office of Basic Energy Sciences, Grant No. DOE FG02-05ER15732) and Nanoholdings LLC for financial support. Use of beamlines X18B, X23A2, and X23B at the National Synchrotron Light Source, Brookhaven National Laboratory, was supported by the U.S. Department of Energy, Office of Science, Office of Basic Energy Sciences, under Contract No. DE-AC02-98CH10886. We are also grateful to Prof. Yuan Chen

and Mr. Li Wei at Nanyang Technological University, Singapore, for the PL and UV−vis−NIR data.

Supporting Information Available: Additional figures. This material is available free of charge via the Internet at http://pubs.acs.org.

References and Notes

(1) Saito, R.; Dresselhaus, G.; Dresselhaus, M. S. *Physical Properties of Carbon Nanotubes*; Imperial College Press: London, 1998.
(2) Weisman, R. B.; Bachilo, S. M. *Nano Lett.* **2003**, *3*, 1235.
(3) Meo, M.; Rossi, M. *Compos. Sci. Technol.* **2006**, *66*, 1597.
(4) Tang, Z. K.; Zhang, L.; Wang, N.; Zhang, X. X.; Wen, G. H.; Li, G. D.; Wang, J. N.; Chan, C. T.; Sheng, P. *Science* **2001**, *292*, 2462.
(5) Tang, Z. K.; Zhang, L. Y.; Wang, N.; Zhang, X. X.; Wang, J. N.; Li, G. D.; Li, Z. M.; Wen, G. H.; Chan, C. T.; Sheng, P. *Synth. Met.* **2003**, *133−134*, 689.
(6) Perfetto, E.; González, J. *J. Phys.: Condens. Matter* **2006**, *18*, S2105.
(7) Wang, X.; Yue, W. B.; He, M. S.; Liu, M. H.; Zhang, J.; Liu, Z. F. *Chem. Mater.* **2004**, *16*, 799.
(8) Alvarez, W. E.; Pompeo, F.; Herrera, J. E.; Balzano, L.; Resasco, D. E. *Chem. Mater.* **2002**, *14*, 1853.
(9) Li, X. L.; Tu, X. M.; Zaric, S.; Welsher, K.; Seo, W. S.; Zhao, W.; Dai, H. J. *J. Am. Chem. Soc.* **2007**, *129*, 15770.
(10) Zoican-Loebick, C.; Derrouiche, S.; Fang, F.; Li, N.; Haller, G. L.; Pfefferle, L. D., submitted.
(11) Yao, M.; Liu, B.; Zou, Y.; Wang, L.; Cui, T.; Zou, G.; Li, J.; Sundquist, B. *J. Phys. Chem. B* **2006**, *110*, 15284.
(12) Smart, S. K.; Cassady, A. I.; Lu, G. Q.; Martin, D. J. *Carbon* **2006**, *44*, 1034.
(13) Dai, X. J.; Skourtis, C. *J. Appl. Phys.* **2008**, *103*, 124305.
(14) Zhang, J.; Liu, X.; Blume, R.; Zhang, A.; Schlögl, R.; Su, D. S. *Science* **2008**, *322*, 73.
(15) Lim, S.; Ciuparu, D.; Pak, C.; Dobek, F.; Chen, Y.; Harding, D.; Pfefferle, L. D.; Haller, G. L. *J. Phys. Chem. B* **2003**, *107*, 11048.
(16) Chen, Y.; Ciuparu, D.; Lim, S.; Yang, Y.; Haller, G. L.; Pfefferle, L. D. *J. Catal.* **2004**, *225*, 453.
(17) Chen, Y.; Ciuparu, D.; Lim, S.; Yang, Y.; Haller, G. L.; Pfefferle, L. D. *J. Catal.* **2004**, *226*, 351.
(18) Ciuparu, D.; Chen, Y.; Lim, S.; Yang, Y.; Haller, G. L.; Pfefferle, L. D. *J. Phys. Chem. B* **2004**, *108*, 15565.
(19) Lim, S.; Ciuparu, D.; Chen, Y.; Yang, Y.; Pfefferle, L. D.; Haller, G. *J. Phys. Chem. B* **2005**, *109*, 2285.
(20) Ciuparu, D.; Haider, P.; Fernandez-Garcia, M.; Chen, Y.; Lim, S.; Haller, G. L.; Pfefferle, L. D. *J. Phys. Chem. B* **2005**, *109*, 16332.
(21) Lim, S.; Wang, C.; Yang, Y.; Ciuparu, D.; Pfefferle, L. D.; Haller, G. L. *Catal. Today* **2007**, *123*, 122.
(22) Lim, S.; Li, N.; Fang, F.; Pinault, M.; Zoican, C.; Wang, C.; Fadel, F.; Pfefferle, L. D.; Haller, G. L. *J. Phys. Chem. C* **2008**, *112*, 12442.
(23) Ago, H.; Imamura, S.; Okazaki, T.; Saito, T.; Yumura, M.; Tsuji, M. *J. Phys. Chem. B* **2005**, *109*, 10035.
(24) Herrera, J. E.; Balzano, L.; Borgna, A.; Alvarez, W. E.; Resasco, D. E. *J. Catal.* **2001**, *204*, 129.
(25) Chen, Y.; Wei, L.; Wang, B.; Lim, S.; Ciuparu, D.; Zheng, M.; Chen, J.; Zoican, C.; Yang, Y.; Haller, G. L.; Pfefferle, L. D. *ACS Nano* **2007**, *1*, 327.
(26) Barrett, E. P.; Joyner, L. G.; Halenda, P. P. *J. Am. Chem. Soc.* **1951**, *73*, 373.
(27) Alvarez, L.; Righi, A.; Guillard, T.; Rols, S.; Anglaret, E.; Laplaze, D.; Sauvajol, J. L. *Chem. Phys. Lett.* **2000**, *316*, 186.
(28) Rao, A. M.; Richter, E.; Bandow, S.; Chase, B.; Eklund, P. C.; Williams, K. A.; Fang, S.; Subbaswamy, K. R.; Menon, M.; Thess, A.; Smalley, R. E.; Dresselhaus, G.; Dresselhaus, M. S. *Science* **1997**, *275*, 187.
(29) Fantini, C.; Jorio, A.; Souza, M.; Saito, R.; Samsonidze, Ge.; Dresselhaus, M. S.; Pimenta, M. Intermediate frequency Raman modes in metallic and semiconducting carbon nanotubes. In *Electronic Properties of Novel Nanostructures*; Kuzmany, H., Fink, J., Mehring, M., Roth, S., Eds.; Springer-Verlag: New York, 2004.
(30) Doorn, S. K.; Luo, Z.; Papadimitrakopoulos, F. *Phys. Status Solidi B* **2007**, *244*, 3992.
(31) Kalbac, M.; Kavan, L.; Zukalova, M.; Dunsch, L. *Phys. Status Solidi B* **2006**, *243*, 3134.
(32) Skakalova, V.; Maultzsch, J.; Osvath, A.; Biro, L.; Roth, S. *Phys. Status Solidi RRL* **2007**, *1*, 138.
(33) Luo, Z.; Papadimitrakopoulos, F.; Doorn, S. *Phys. Rev. B* **2008**, *77*, 035421.
(34) Bachilo, S. M.; Strano, M. S.; Kittrell, C.; Hauge, R. H.; Smalley, R. E.; Weisman, R. B. *Science* **2002**, *298*, 2361.
(35) Wang, B.; Poa, C. H. P.; Wei, L.; Li, L.-J.; Yang, Y.; Chen, Y. *J. Am. Chem. Soc.* **2007**, *129*, 9014.
(36) Newwille, M. *J. Synchrotron Radiat.* **2001**, *8*, 322.
(37) Ravel, B.; Newville, M. *J. Synchrotron Radiat.* **2005**, *12*, 537.
(38) Calvin, S.; Luo, S. X.; Caragianis-Broadbridge, C.; McGuinness, J. K.; Anderson, E.; Lehman, A.; Wee, K. H.; Morrison, S. A.; Kurihara, L. K. *Appl. Phys. Lett.* **2005**, *87*, 233102.
(39) Ushiro, M.; Uno, K.; Fujikawa, T.; Sato, Y.; Tohji, K.; Watari, F.; Chun, W.-J.; Koike, Y.; Asakura, K. *Phys. Rev. B* **2006**, *73*, 144103.
(40) Rege, S. U.; Yang, R. T. *AIChE J.* **2000**, *46*, 734.
(41) Wang, C.; Lim, S.; Du, G.; Zoican-Loebick, C.; Li, N.; Derrouiche, S.; Haller, G. L. *J. Phys. Chem. C,* in revision.
(42) Kang, S.; Pinault, M.; Pfefferle, L. D.; Elimelech, M. *Langmuir* **2007**, *23*, 8670.
(43) Fadel, T. R.; Steenblock, E. R.; Stern, E.; Li, N.; Wang, X.; Haller, G. L.; Pfefferle, L. D.; Fahmy, T. M. *Nano Lett.* **2008**, *8*, 2070.

JP903129H